EUROPEAN ORGANIZATION FOR NUCLEAR RESEARCH

CERN-PPE/93-159
27 August 1993

DESIGN CHOICES AND ISSUES IN FIXED-TARGET B EXPERIMENTS

LESLIE CAMILLERI
PPE Division, CERN
1211 Geneva 23, Switzerland

Plenary talk given at the
Worshop on B Physics at Hadron Accelerators
June 21–July 2, 1993
Snowmass, Colorado, USA

1. THE PHYSICS MEASUREMENTS

1.1 CP Violation

The main priority of any experiment on B physics in the years to come will be an endeavour to observe CP violation in the B sector [1]. This can be attempted in several ways as described in the theoretical talks in this workshop.

a) A measurement of the CP asymmetry

$$A = \frac{\left(\overline{B}^0 \to f\right) - \left(B^0 \to f\right)}{\left(\overline{B}_0 \to f\right) + \left(B^0 \to f\right)},$$

where f is a self-conjugate state, will yield a measure of the angles α, β, and γ through a measurement of $B_d^0 \to \pi^+\pi^-$, $B_d^0 \to \psi K_S^0$, and $B_s^0 \to \rho^0 K_S^0$ respectively. In order to determine whether the observed decay originated from a B^0 or a $\overline{B}^0$, the nature of the companion B must be ascertained, most probably through the sign of the lepton or the kaon it decays to. A measurement of these three angles will overconstrain the unitary triangle shown in Fig. 1.

b) The angle γ can also be determined by measuring six self-tagging reactions [2].

$$B_d^0 \to \overline{D}^0 K^{*0},\ D^0 K^{*0},\ D_1^0 K^{*0} \quad \text{and} \quad \overline{B}_d^0 \to \overline{D}_0 K^{*0},\ D^0 \overline{K}^{*0},\ D_1^0 \overline{K}^{*0},$$

where D_1^0 denotes the decay of a D^0 into CP eigenstates, such as $\pi\pi$, $\pi\pi\pi\pi$, KK, and KK$\pi\pi$. Constructing the triangles shown in Fig. 2 will yield a measurement of γ. Note that all six reactions are characterized by at least four tracks not coming from the primary vertex.

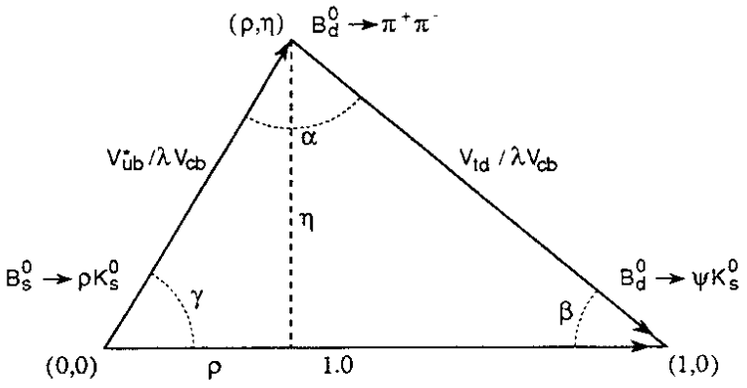

Figure 1. The unitary triangle.

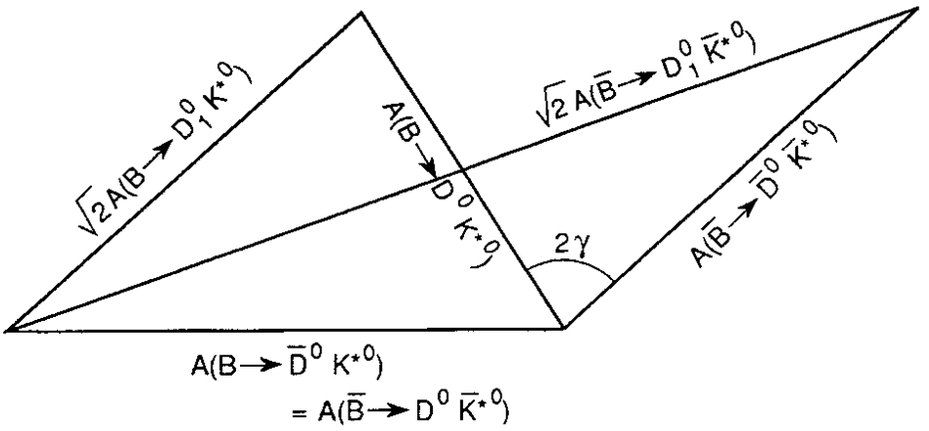

Figure 2. Self-tagging processes arranged in two triangles giving the angle γ.

1.2 B_s^0 *Oscillations*

These are expected to be very fast and hadron machines may well be the only way to observe them. They could be observed in the decay

$$B_s^0 \to D_s^{\pm}\pi^{\mp}$$
$$\hookrightarrow \phi\,\pi^{\pm}$$
$$\hookrightarrow K^+K^-$$

Here again the reaction involves four tracks originating at secondary vertices. At LHC fixed-target conditions ($\sqrt{s}$=114 GeV) the oscillation length is of the order of 1 cm for $x_S \approx 12$. Vertex resolutions of $\approx$ 1 mm are therefore needed.

1.3 *Rare Decay Modes*

The inclusive reactions $B \to \mu^+\mu^- X$ and $B \to e^+e^- X$ as well as the exclusive channels $B \to \mu^+\mu^-$ and $B \to e^+e^-$ could be observed using a lepton trigger. In the latter case the Standard Model predicts [3] a branching ratio of $\sim 10^{-9}$. Any deviations from this number could point to new physics. For instance a two Higgs Doublet extension would predict [4] a branching ratio of 10^{-8} for $m_t \approx 150$ GeV/c^2, $m_H < 400$ GeV/c^2, and small tan β.

1.4 *Tagging*

For those reactions which are not self-tagging the nature of the companion B must be determined. Experimentally this is most easily done by determining the sign of the lepton in its semi-leptonic decays. However, this is costly in event numbers as only 21% of the B's decay to an electron or a muon. Furthermore, mistags can occur because of the observed leptons originating from the $B \to D \to$ ⁻ chain, from π/K decays, or from π/μ or π/e misidentifications. These mistags can be reduced by requiring the lepton to have $p_T > 1.2$ GeV/c. The efficiency of this cut is 0.8 for B's and results in

$$\omega = \frac{\text{wrong tags}}{\text{all tags}} = 0.17.$$

The nature of the companion B can also be determined by measuring the sign of the charged kaon in the $B \to D \to K$ chain. More events are retained this way as 50% of the B's result in a charged kaon. Mistags are due to $B \to D\overline{D}$ decays and Cabibbo suppressed decays. For kaons $\omega = 0.16$.

In principle, it is also possible to tag by directly measuring the charge of the companion $B^{\pm}$, either in a very strong magnetic field or by reconstructing all the decay charged particles.

Finally, as explained in an earlier talk, the effect of oscillations of the companion B results in a value of

$$\overline{\omega} = \frac{\text{wrong tag}}{\text{all tag}} = 0.25.$$

1.5 *Checks*

Because the initial state is pp rather than $\bar{p}p$, the B^0 and $\overline{B}^0$ production rates will not necessarily be the same [5]. Before a CP asymmetry can be measured these production rates will, of course, have to be known. This can be done by measuring the reactions

$$B^0 \to J/\psi K^* \qquad \overline{B}^0 \to J/\psi \overline{K}^*$$
$$\hookrightarrow K^+\pi^- \qquad\qquad \hookrightarrow K^-\pi^+$$

These reactions are expected to have a branching ratio that is three times bigger than the $J/\psi K_S^0$ decays and they will of course be automatically included in a J/ψ trigger. Furthermore, they are not expected to exhibit CP violation and they are self tagging. Because of this latter property an observation of this reaction will yield a measurement of dilution effects in "companion B tagging".

The production rates for B^+ and B^- will also need to be known in order to compute $\overline{\omega}$. Here the reaction $B^{\pm} \rightarrow J/\psi K^{\pm}$, which will also be included in a J/ψ trigger, can be used.

Both these reactions will need particle identification.

These measurements imply the following requirements of the experiment.

a) *Trigger*
- A muon trigger will be sensitive to J/ψ reactions and muon tags.
- An electron trigger will double the number of lepton events.
- In order to include kaon tags and self-tagging reactions, the experiment must not rely entirely on lepton triggers. Secondary vertex triggers and hadron p_T triggers should be included in order to have the maximum flexibility.

b) *Detector*
- Vertex detector.
- Particle identification.
- Good momentum resolution.
- Electromagnetic and hadronic calorimeters.
- Muon detector.

2. QUESTIONS AND ISSUES

The following issues have to be addressed.

- Collider or fixed-target mode?
- If fixed target, extracted beam or internal target?
- If internal target, gas jet or wire target?
- If a gas jet, hydrogen or a heavy gas?
- Beam pipe design.
- Silicon microvertex design and radiation damage.
- K_S^0 decay path.
- Particle identification.
- Momentum resolution.
- Order of detectors.

2.1 Collider or Fixed Target

- The mean B flight path is much longer in a fixed-target mode than in a collider mode (Fig. 3). Furthermore, the target region in fixed-target can be limited to a few millimetres compared with several centimetres in a collider mode. This makes for much easier separation of a secondary vertex from the primary vertex, even at the trigger level.
- Owing to the lower $\sqrt{s}$ in fixed-target mode, the associated multiplicity is lower (Fig. 4). Comparing a fixed-target spectrometer having an acceptance of 3.5–87 mrad with a forward collider [6] one having an acceptance of 5–600 mrad, the mean charged multiplicity associated with a B is 9.5 as against 30.3 and the mean number of associated K_S^0 is 0.9 as against 1.9.
- Whereas the p_T distribution of secondaries from B decays is the same for fixed-target and collider modes, the p_T distribution of minimum bias events is much steeper in fixed-target than in collider modes. This results in a hadronic p_T trigger having a rejection of 6×10^{-4}

against minimum bias events in fixed-target mode and only 5×10^{-2} in collider mode for an efficiency for $B \rightarrow \pi^+\pi^-$ of 0.80 in both cases.

– The momenta are higher in fixed-target mode resulting in less multiple scattering.

– In the case of an extracted beam there is no need for a beam pipe or roman pots.

But of course the cross-section [7] is smaller in fixed-target mode by a factor of 500 and the signal to noise ratio is also worse by a factor of 200.

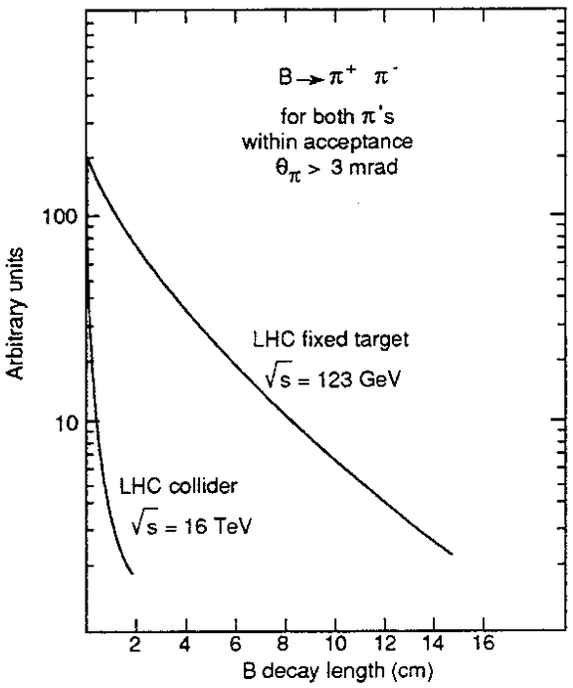

Figure 3. The decay path distributions of B mesons decaying to $\pi^+\pi^-$ for fixed-target and collider modes at the LHC. The π^+ and π^- are required to have a production angle greater than 3 mrad.

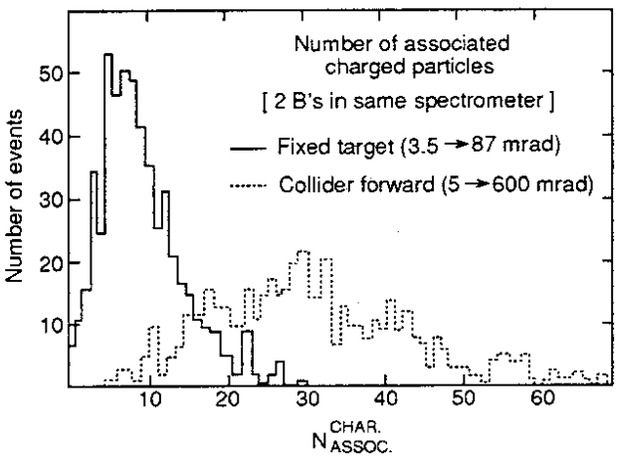

Figure 4. The charged-particle multiplicity associated with B mesons for fixed-target (3.5–87 mrad) and collider (5–600 mrad) geometries at the LHC.

2.2 *Extracted Beam*

At the LHC and SSC a continuously extracted beam can be obtained using channeling by a bent crystal placed in the halo of the beam. The halo particles are guided by the bent crystal planes and deviated by ~ 0.7 mrad. The principle was tested [8] using a 120 GeV beam at the CERN SPS. The counting rate in a counter telescope is shown in Fig. 5 as a function of crystal orientation. A clear peak is observed. Channeling efficiencies of 10–12% have been measured. Both the SFT [9] and LHB [10] proposals intend to use this technique.

Table 1 is a summary of running or proposed extracted beam B experiments. It can be seen that the longitudinal target dimension varies from 0.2 cm to 18 cm and that the target thicknesses are several tens of per cent of a radiation length and several per cent of an interaction length. This results in many conversions and secondary interactions thus increasing the multiplicity in an event and producing "fake" secondary vertices. The beam intensities vary from 2.5×10^6 to 4×10^9 particles per second (2×10^8 for SFT and LHB)

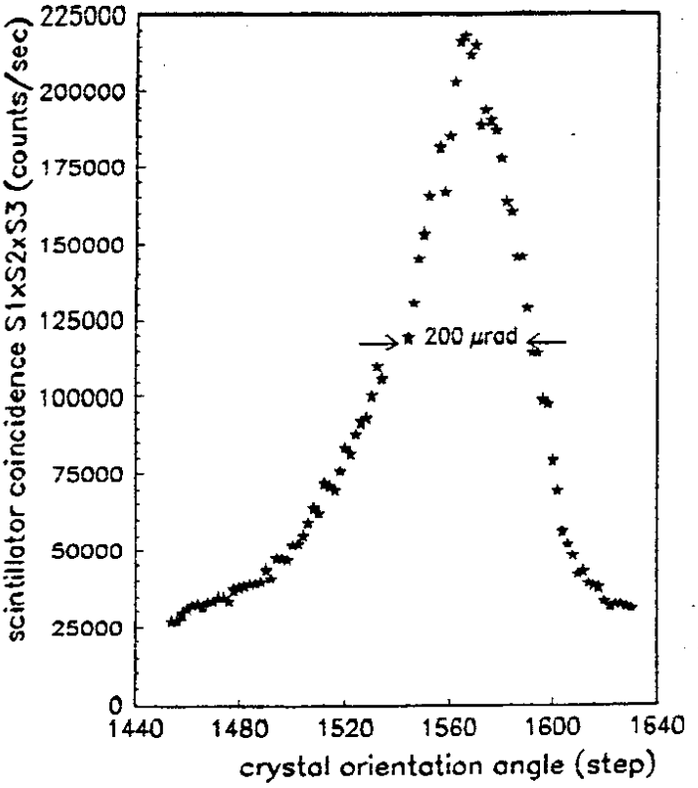

Figure 5. The counting rate in a scintillator counter telescope
as a function of crystal orientation in a bent crystal extraction test at the SPS.

Table 1. A summary of extracted beam experiments.

Experiment	Beam intensity (protons/s)	Target Type	($\%X_0$)	($\%\lambda_{int}$)
WA92 [11]	$2.5 \times 10^6(\pi^-)$	2 mm Cu	14	1.3
E771 [12]	4.6×10^7	24 mm Si	25	4.1
E789 [13]	3.0×10^9 [During flat top]	3 mm W	86	3.1
P865 [14]	4×10^9 [During flat top]	2 mm W	57	2.1
P867 [15]	1.2×10^8	24 mm Si	25	4.1
SFT [9]	2×10^8	18 mm Si 90 planes over 18 cm	19	7.7
LHB [10]	2×10^8	7.5 mm Cu	52	5

2.3 Internal Target

2.3.1 Gas jet

An experiment using a gas jet in the circulating beam of a collider uses a beam of

EFFECTIVE INTENSITY = NUMBER OF CIRCULATING PROTONS × REVOLUTION FREQUENCY
$= (1.5 \times 10^{14}) \times 3441 = 5.2 \times 10^{17}$ p/s at SSC
$= (4.8 \times 10^{14}) \times 11246 = 5.4 \times 10^{18}$ p/s at LHC.

This is ten orders of magnitude more than an extracted beam and therefore allows the use of a very thin target such as a gas jet. This in turn implies no conversions, no secondary interactions, and no multiple scattering in the target.

A molecular hydrogen cluster target has been used [16] for seven years in the SPS collider by experiment UA6. The design is shown in Fig. 6. Hydrogen gas is pumped through a 0.1 mm nozzle cooled to 25 K. Saturation occurs on the other side of the nozzle and clusters of ~ 10^5 molecules are formed. This cluster jet is collimated using a skimmer and diaphragms. It then traverses the circulating beam and is absorbed in a cryopump. In UA6 the jet profile at the beam was 2.5 mm transverse to the beam and 8 mm along the beam, and its density was 4×10^{14} p/cm^3. The integrated density along the beam was 3.2×10^{14} p/cm^2. For use in the proposed GAJET B experiment [17] the longitudinal dimension of the jet must be reduced to about 2 mm, while maintaining approximately the same integrated density. This can be done by reducing the size of the diaphragm and skimmer holes, reducing the distance between the nozzle and the circulating beam from 22 cm to 13 cm, and increasing the gas throughput by a factor of 1.7. This should result in a 2 mm long jet with an integrated density of 3.8×10^{14} p/cm^2. It must be ascertained that no diffuse gas remains in the vicinity of the jet. The upper limit on this number from UA6 is 5% of the peak density.

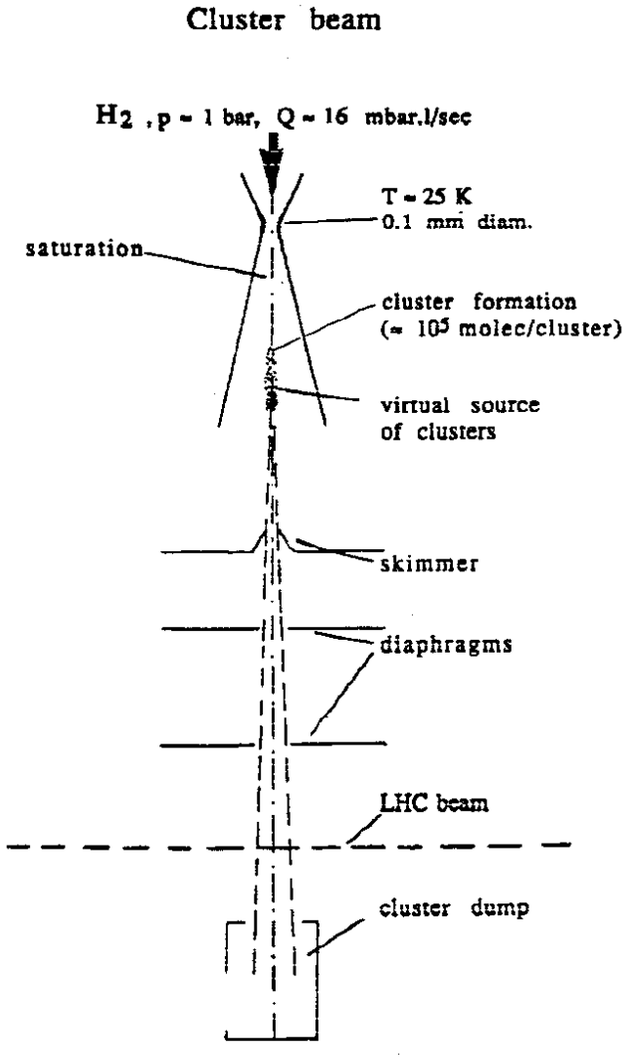

Figure 6. The UA6 molecular cluster jet design.

2.3.2 Wire target

This is a method advocated by the proponents of the HERA B experiment [18]. Eight 50 μm steel wires would be placed in the halo of the 820 GeV proton beam at about 4 beam σ's from the centre. They would be arranged in two groups of four wires 5 cm apart, as shown in Fig. 7. A wire target is favoured by this group over a gas jet as it only affects the particles in the halo, which are in any case lost to the main ep experiments; it needs a simple scraper type mechanism rather than big pumping stations and it produces no diffuse gas. However, a sudden movement of the beam could result in large increases in counting rates, whereas with a gas jet a movement of the beam can only reduce the counting rate. The technique was tested with a single wire and was shown to produce stable counting rates five minutes after moving the wire into position. Also, no background increase was observed in the ep experiments.

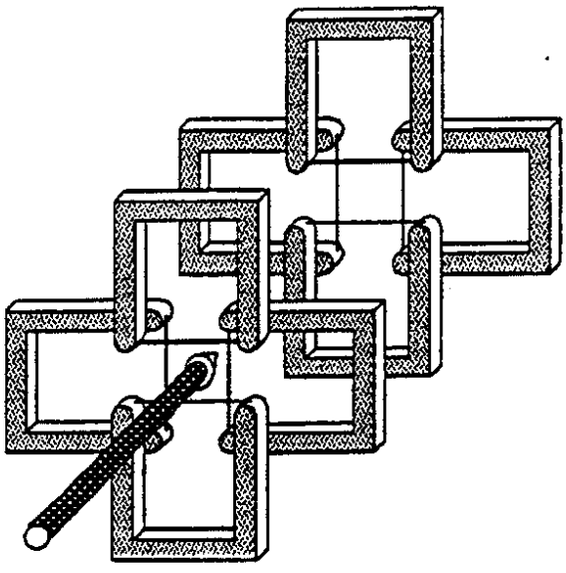

Figure 7: The eight-wire configuration of the HERA B proposed internal target.

2.4 The Use of Heavy Gases in a Jet

The following applies to metallic targets as well. It is expected that the $B\overline{B}$ production cross-section will be proportional to A^{α}, where A = atomic weight of the target and $0.9 < \alpha < 1.0$. On the other hand, the total cross-section is known to be proportional to $A^{0.72}$. The ratio of the $\sigma_{B\overline{B}}$ to σ_{tot} will therefore be F times what it is in hydrogen where $F = A^{\alpha-0.72}$. For argon (A = 40) and $\alpha = 0.95$, F is equal [19] to 2.3. Therefore, for a given number of minimum bias events there will be 2.3 times more $B\overline{B}$ events in argon than in hydrogen. Hence a better signal-to-noise ratio for $A \neq 1$ targets.

There is however a price to pay.

- Both the multiplicity associated with a $B\overline{B}$ pair and the multiplicity in minimum bias events are about a factor of 2 higher in pA collision than in pp collisions, thus increasing the complexity of events [20].
- In pA collisions the production cross-section for pions [21] of $p_T > 2.0$ GeV/c is proportional to $A^{1.15}$. As an example, for a copper target (A = 64) the cross-section for pion production per nucleon is 1.9 times bigger than the pp cross-section. The difference in p_T distribution between minimum bias events and B events is thus reduced in pA collisions.

A summary of the luminosities, interaction rates, and numbers of minimum bias events per bunch is given in Table 2 for SFT, LHB, GAJET, and HERA B. The number of interaction rates varies from 0.1 per bunch for SFT to 4.0 per bunch for HERA B.

Table 2. Cross-sections, luminosities and interaction rates for proposed fixed-target experiments on CP violation.

	$\sigma_{B\overline{B}}$ per nucleon (μb)	σ^{pA}/A = effective σ^{inel} per nucleon (mb)	Luminosity	Interaction rate (MHz)	Bunch spacing (ns)	Min. bias events per bunch
SFT	1.5	14	5×10^{32}	7	16	0.1
LHB	1.0	11	8×10^{32}	9	25	0.2
GAJET	1.0	35	2×10^{33}	70	25	1.8
HERA B	0.01	10	4×10^{33}	40	100	4.0

2.5 *Beam Pipe Design*

For experiment using an internal target, the B decay products must traverse the storage ring beam pipe. It must therefore be carefully designed to minimize the amount of material. In particular, heavy flanges and septum plates must be avoided. Glancing incidence on even very thin pipes can result in traversals of several radiation lengths of material [22]. The silicon microvertex detector must be housed inside the beam pipe in roman pots.

2.6 *Silicon Microvertex Detector*

In the case of experiments using an external beam, the microvertex detector can be placed immediately following the target (LHB) or can actually constitute the target (SFT). In both cases the B's have enough flight path to decay within the microvertex detector. This makes the pattern recognition problem much easier, as demonstrated by the WA92 experiment at CERN [23]. The direct observation of decay vertices within the microvertex detector is a distinct advantage of an extracted beam over all other methods of studying B production.

The SFT active target design consists of 90 planes of 200 μm thick silicon planes spread over 18 cm along the beam and followed by further reconstruction planes occupying 120 cm along the beam.

For a gas jet target or a wire target the silicon planes must be housed in roman pots. The minimum distance of approach to the beam, dictated either by radiation dose or by disturbance to the beam, together with the minimum production angle to be observed determines the position of these detectors along the beam. In the case of GAJET the detectors consists of nine 300 μm thick double sided reconstruction planes of 25 μm pitch. These reconstruction planes, together with six additional trigger planes, are located at distances varying between 40 cm and 400 cm from the jet. They can be located in individual pots or grouped in a few pots following the design pioneered by P238: partial vacuum within the pots allows very thin walls [24]. The decay vertices can be reconstructed with a precision of ± 1 mm along the beam and ± 20 μm transverse to the beam.

2.7 *Radiation Damage to the Silicon Microvertex*

The radiation dose, D, absorbed in 10^7 s by a strip located at a distance of R cm from the beam is given by [25]

$$D = 2.66\times10^{-14}\Phi$$
$$= 4.2\times10^{-13} + \sigma_{tot}\frac{dN}{d\eta}\cdot\frac{1}{R^2} \text{ MRad}$$

where

Φ = fluence (particles per cm^2)
+ = instantaneous luminosity
σ_{tot} = total cross-section
$dN/d\eta$ = number of particles per unit of rapidity.

The dose is essentially independent of the distance ALONG the beam at which the detector is placed but depends critically on the transverse distance R from the beam. For a given luminosity, the maximum dose tolerable [26] by the silicon will determine the minimum distance R_{min} at which the detectors can be placed. For a desired angular coverage, this in turn will fix the distance along the beam at which the detectors must be placed.

As an example, for GAJET running at 2×10^{33} cm^{-2} s^{-1} a dose of 20 MRad/year is expected for a strip 7 mm from the beam.

In the case of an extracted beam there is an extra complication because, in order to capitalize on the fact that in these experiments the B decay vertex can occur within the vertex detector, the beam must also go through the vertex detector. This would quickly destroy the silicon at the spot traversed by the beam. The solution is to spread the radiation damage due to the beam over an area S cm^2. The LHB solution is to move the vertex detector over an area of 10×10 cm^2, whereas SFT intends to use a beam of 8 cm diameter. Either solution necessitates a vertex detector of much larger dimensions than would be needed with a fixed narrow beam. The fluence is than given by [25].

$$\Phi = (10^7 s)\,(N_p) \times (1 + L_T \langle N_{ch} \rangle f_{pA}\, f_{SI})/s$$

where

N_p = Number of protons per second in the beam
L_T = Target thickness in units of interaction length
$\langle N_{ch} \rangle$ = Mean number of charged particles per interaction
f_{pA} = Nuclear enhancement of multiplicity ≈ 2
f_{SI} = Enhancement of multiplicity due to secondary interactions and conversions ≈ 2.

A comparison of LHB with GAJET, both at a luminosity of 10^{33} cm^2 s^{-1}, results in LHB expecting a dose of 2.4 MRad everywhere, whereas GAJET expects a maximum of 7.5 MRad at 0.7 cm from the beam. The extracted beam experiment expects a smaller maximum dose because of its ability to spread the radiation damage of the beam over a large area.

2.8 K^0_S Decay Region

It is necessary to allow a significant distance for the K^0_S to decay before the magnetic analysis. The mean decay length at the LHC fixed target is 8.6 m. In order to maximize the distance available for K^0_S decay GAJET is investigating the possibility of installing the RICH in front of the magnet.

2.9 Particle Identification

Discrimination between pions and kaons is necessary for kaon tagging and to avoid the contamination of the $B \rightarrow \pi\pi$ sample by $B \rightarrow K\pi$ decays. The latter is the most difficult problem because of the high momenta of the pions in $B \rightarrow \pi\pi$ events (Fig. 8). Rejecting candidate events with momenta larger than 250 GeV/c would result in an efficiency of only 50%. Extending the upper momentum cut to 600 GeV/c would recover most of the lost events.

The SFT Collaboration proposes to use a 12 m long neon-filled RICH. The Cherenkov photons are to be observed in an array of multianode photomultipliers. These are preferred over TEA or TMAE filled wire chambers because of

– small (< 2 ns) dispersion in collection time
– no need for high temperature or low pressure
– no need for ultra-pure radiator gas (TEA is only sensitive to UV photons and hence is very sensitive to oxygen contamination).

The upper limit in momentum for π/K discrimination at the 2 standard deviation level is shown in Fig. 9 as a function of anode pad size. It can be seen that discrimination can be obtained for momenta up to 300 GeV/c for a pad size of 3×3 mm^2.

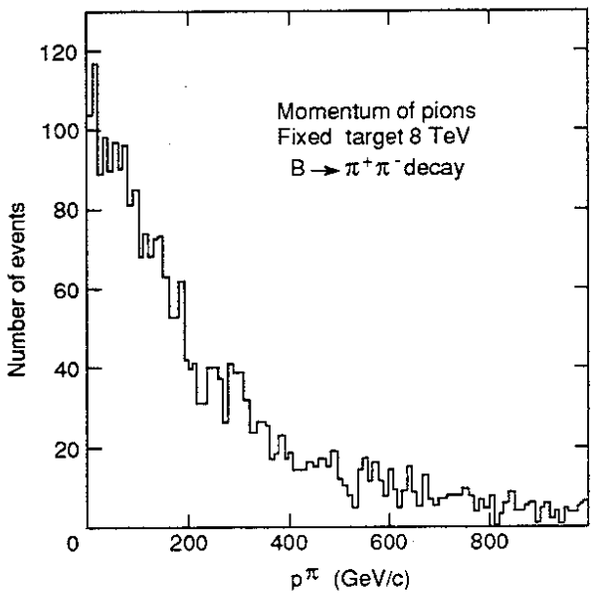

Figure 8. The momentum distribution of π's from $B \rightarrow \pi^+\pi^-$ in a LHC fixed-target mode.

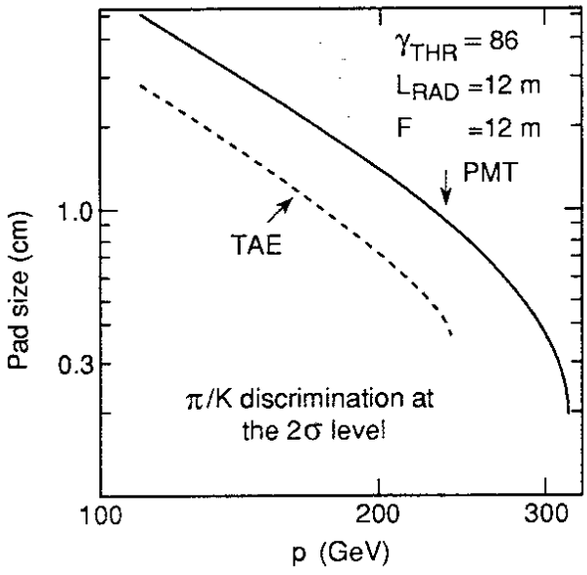

Figure 9. The momentum up to which pions and kaons can be separated as a function of the pad size of the multianode photomultiplier used to detect the Cherenkov photons.

Another very interesting new idea, currently being investigated by P865, is the use of Visible Light Photon Counters instead of phototubes or wire chambers.

Beyond these momenta it should be possible to use transition radiation detectors for π/K separation. GAJET is proposing to use 100 modules of the type developed for ATLAS in the RD6 project [27]. Each module consists of 12 $\times$ 15 μm thick polypropylene foils separated by 370 μm and of one plane of 4 mm diameter Xe-filled straw tubes separated by 8 mm. Defining a "hit" as a tube containing an energy deposition greater than 5 keV (where a minimum ionizing particle deposits 1.8 keV), the distribution of the number of hits along a track is plotted for pions and kaons of 400 GeV/c (Fig. 10a). The particles cannot be distinguished at low momenta, where both of them do not give transition radiation and at very high momenta where both of them do. However, between 150 and 450 GeV/c a kaon suppression factor of 10 can be obtained (Fig. 10b).

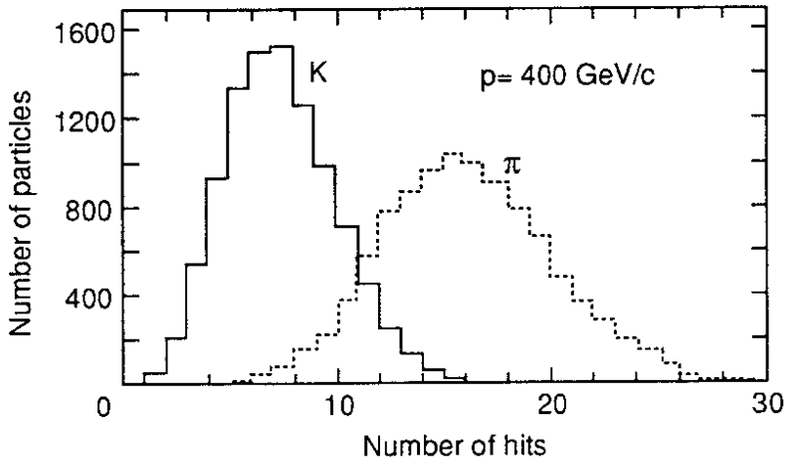

Figure 10a. The distribution of hits in a 100 plane TRD for pions and kaons of 400 GeV/c momentum.

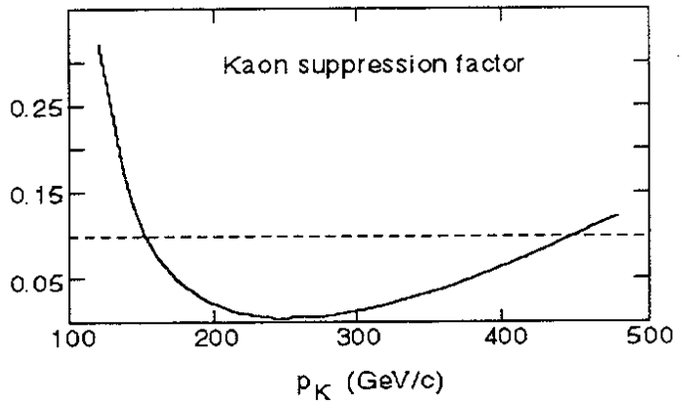

Figure 10b. The kaon suppression factor provided by the TRD as a function of momentum.

2.10 The magnetic spectrometer

It is expected that it will not be possible to link observed π^0's to a given decay vertex. It is therefore important to be able to distinguish between $B \rightarrow \psi K_S^0$ and $B \rightarrow \psi K_S^0 \pi^0$ on the basis of the reconstruction of the ψ and the K_S^0 only. The ψK_S^0 invariant mass for the two modes is shown in Fig. 11 for a momentum resolution $\sigma_p/p = 10^{-4}$ p. For this momentum resolution the background for $\psi K_S^0 \pi^0$ under the peak from ψK_S^0 is small. However, worsening the momentum resolution would clearly broaden the peak and move more background to higher masses. Similarly for $B \rightarrow \pi^+\pi^-\pi^0$ and $B \rightarrow \pi^+\pi^-$.

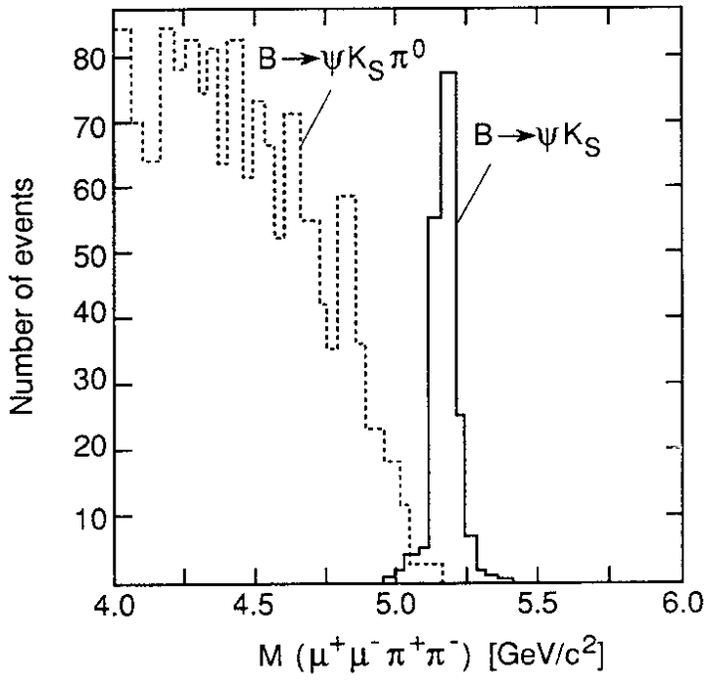

Figure 11. The invariant mass of ψK_S^0 for $B \rightarrow \psi K_S^0$ and $B \rightarrow \psi K_S^0 \pi^0$ assuming a momentum resolution of $\sigma(p)/p = 10^{-4}$ p.

2.11 Order of Detector Components

Several possibilities can be envisaged. GAJET, HERA B, P865 and P867 envisage the use of a single magnet, whereas SFT and LHB are thinking of two. As mentioned earlier, GAJET is advocating placing the RICH before the magnet unlike the other proposals. This maximizes the K_S^0 decay volume, and results in straight tracks from a point source in the RICH. In this configuration the magnet is closer to the calorimeter thus minimizing the effect of the magnetic bend on the p_T of a particle as calculated from calorimeter information alone.

3. FIRST-LEVEL TRIGGERS

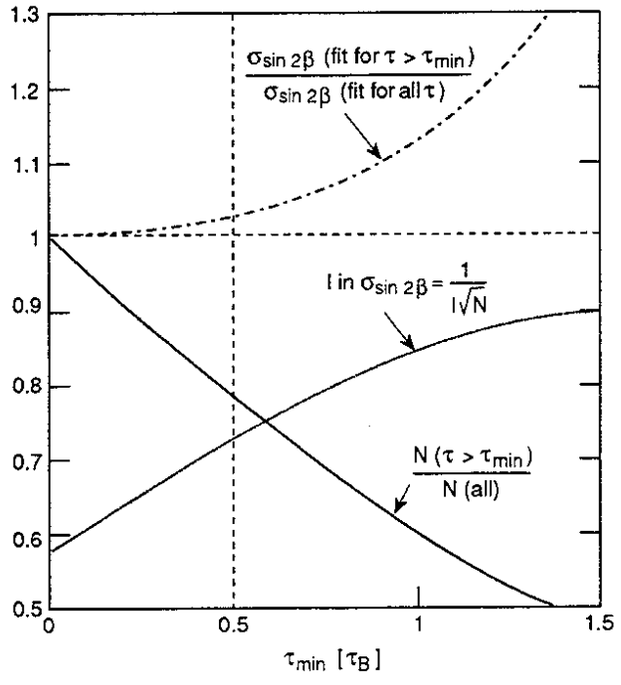

Figure 12. The proportion of the number of events retained, the fitting factor I, and the degradation in the error in sin 2β as a function of the lowest value of proper time, τ_{min}, used in the analysis.

It is assumed that the data will be pipelined over about 2.5 μs and that the first-level triggers should give a rejection of about 1000 in that time. Four types of triggers will be discussed – an optical discriminator, a silicon trigger, a p_T trigger, and a muon trigger. The first two select events with tracks not originating at the target and give rejections which are therefore correlated. In selecting events with a displaced second vertex, these two triggers necessarily reject B decays at small proper time. However, the CP asymmetry of these events is small and therefore rejecting them does not significantly worsen the error on the asymmetry. This is demonstrated in Fig. 12, which shows, as a function of the lower cut of the proper time τ_{min}, the number of events retained, the error on the asymmetry, and the fitting factor I, all normalized by their value at $\tau_{min} = 0$ (all events retained). For a cut at $\tau > 0.5\ \tau_B$, 22% of the events are lost but the error only worsens by 2%. This is therefore a useful cut.

3.1 The Optical Discriminator [28]

It consists of a shell of transparent material centred on the target. The index of refraction of the material is chosen such that Cherenkov light emitted in the shell by charged particles originating at the target is refracted out, whereas some of the light emitted by particles not pointing to the target is trapped in the shell by total internal reflection and emerges at the edge of the shell (Fig. 13). The principle was tested [29] by placing a LiF shell in a parallel beam (Fig. 14). For each particle a pseudo-impact parameter, b, could be calculated. It increased with distance from the middle of the crystal. The mean number of photoelectrons observed at the edge of the shell is plotted in Fig. 15 as a function of b. It can be seen that, as expected, very little light is trapped and collected at the edge for particles with b = 0 (i.e. particles simulating those originating from the target). Furthermore, the amount of collected light increases with b. However, it is obvious from the figure that the device tested is only sensitive to impact

parameters above ~ 4 mm, whereas in a B experiment an optical discriminator must be able to trigger on impact parameters of a few hundred microns. The result of a Monte Carlo calculation which includes Fresnel reflection, refraction, chromaticity mirror collection efficiency, and quantum efficiency of the photomultiplier is also shown in Fig. 15 and agrees very well with the data. This program was therefore used to predict the behaviour of different optical configurations. For a shell of index of refraction n_1, immersed in a medium of index n_2, the condition NOT to collect light for particles with b = 0 is

$$1-\left(n_1^2-n_2^2\right)>0\,.$$

The closer this quantity is to zero the smaller will be the impact parameters that result in collected light. Furthermore, in order to obtain a sharp threshold and a large amount of collected light, this condition must be satisfied by as large a range of wavelengths as possible. Such an achromatic combination of n_1 and n_2 would be obtained with sapphire ($A1_2O_3$, n_1 = 1.8) coated with $Si0_2$ (n_2 = 1.5). For small impact parameters only light emitted in the last part of the shell is trapped. The amount of collected light can therefore be increased by replacing a single thick shell by several thinner concentric achromatic shells. The efficiency for retaining $B \rightarrow \pi^+\pi^-$ and minimum bias events as a function of a cut on the number of observed photoelectrons, N_{opt}, was calculated using the Monte Carlo described earlier, for the GAJET geometry (Fig. 16). An efficiency for $B \rightarrow \pi^+\pi^-$ of 0.62 and for minimum bias of 0.1 was obtained for $N_{opt} \geq 8$. This trigger has a very fast response time ~ 25 ns and could even give a decision in less than the bunch crossing time. It relies heavily on having a point target. Its rejection of minimum bias events worsens by a factor of 3 in going from a 2 mm long to a 7 mm long target because of minimum bias events produced at the edges of the target simulating $b \neq 0$ events.

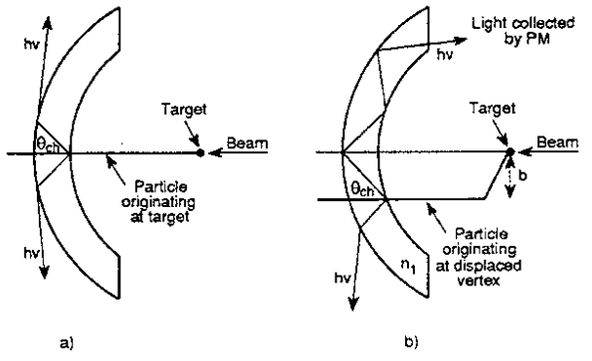

Figure 13: The principle of the optical discriminator. a) Cherenkov light refracted out of the shell for a particle originating at the target. b) Some Cherenkov light totally internally reflected to the edge of the shell for a particle not originating at the target.

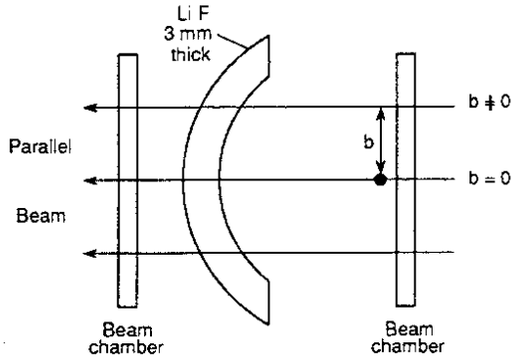

Figure 14. Test of an optical discriminator in a parallel beam. The off-axis particles simulate particles not originating at the target.

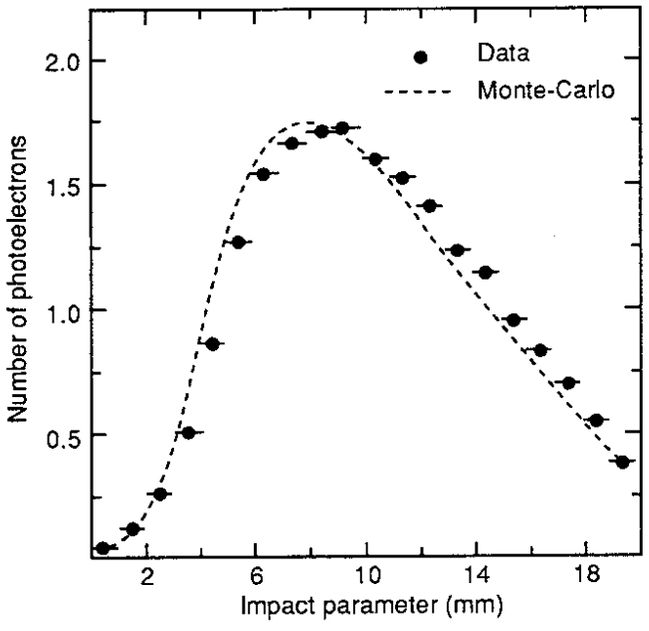

Figure 15. The mean number of photoelectrons as a function of impact parameter for data and Monte Carlo.

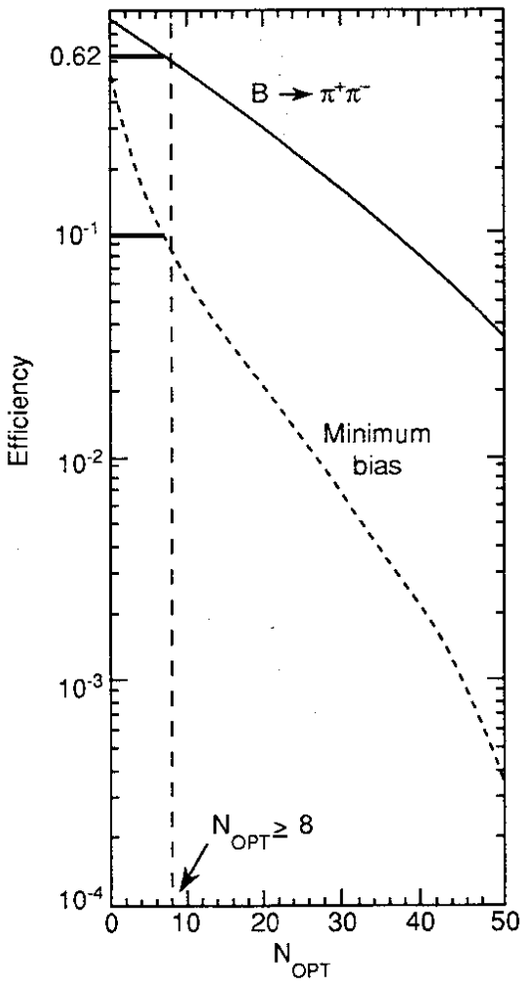

Figure 16. The efficiency of the optical trigger as a function of the lower cut on the number of detected photoelectrons for $B \rightarrow \pi^+\pi^-$ and for minimum bias.

3.2 Secondary Vertex Trigger

This would be based on silicon planes. For experiments with point targets (gas jets or wire targets) in which the primary vertex is automatically known, the preferred geometry to capitalize on the long flight path of the B is an r–Φ geometry. To reduce combinatorial background, each r–Φ strip can be divided into striplets. The trigger could be based on 3 planes, the number of striplets in each plane being the same but their dimensions increasing in proportion to the distance of the plane from the target. Thus a track originating at the target will intersect striplets of the same order number in the 3 planes and can be easily rejected. The trigger algorithm would

- reject hits that form 3-hit combinations, pointing to the target;
- form 3-hit combinations that point downstream of the target;
- require at least 3 such combinations.

A Monte Carlo program which includes multiple scattering indicates that a rejection of minimum bias events by more than a factor of 100 can be obtained for a 50% B efficiency. It is expected that this rejection can be obtained in less than 2.5 μs.

3.3 *Transverse Momentum Trigger for Hadrons and Electrons*

The energy and position information to form the p_T trigger can be obtained:

- either from the calorimeter; this is fast but has a worse resolution and is affected by the magnetic deflection;
- or from pad chambers and the magnet; this is slower and is affected by chamber occupancy; however, it is more accurate and computes the true p_T.

It may be that the best solution would be to use the magnetic bend algorithms in which the position information of the last pad plane is replaced by position information obtained from the calorimeter. The following calculation is based on calorimeter information only in the GAJET geometry.

An individual calorimeter cell (4×4 cm^2) consists of a scintillator tile S_1, 2 X_0 of lead, a scintillator tile S_2, an electromagnetic calorimeter cell of lead scintillator tile design, a hadron calorimeter cell. Using appropriate combinations of S_1, S_2, an electromagnetic cell and a hadronic cell, we can define signatures for charged hadrons, electrons, and photons. Overlapping clusters of 3×3 cells for electrons and 5×5 cells for hadrons can be formed. A Monte Carlo which includes multiple interactions, calorimeter resolutions, and the effect of the magnetic bending results in the efficiencies for triggering on a single hadronic cluster of $p_T \geq p_T^{HADR}$ shown in Fig. 17. In GAJET for $p_T^{HADR} > 2.6$ GeV/c the efficiency for $B \rightarrow \pi^+\pi^-$ is 54% to be compared with 0.9% for minimum bias events. The trigger efficiencies are 96% for $B \rightarrow J/\psi K_S^0$, $J/\psi K_S^0 \rightarrow e^+e^-$ compared with 1.7% for minimum bias events when triggering on $p_T^{elec} > 1$ GeV/c.

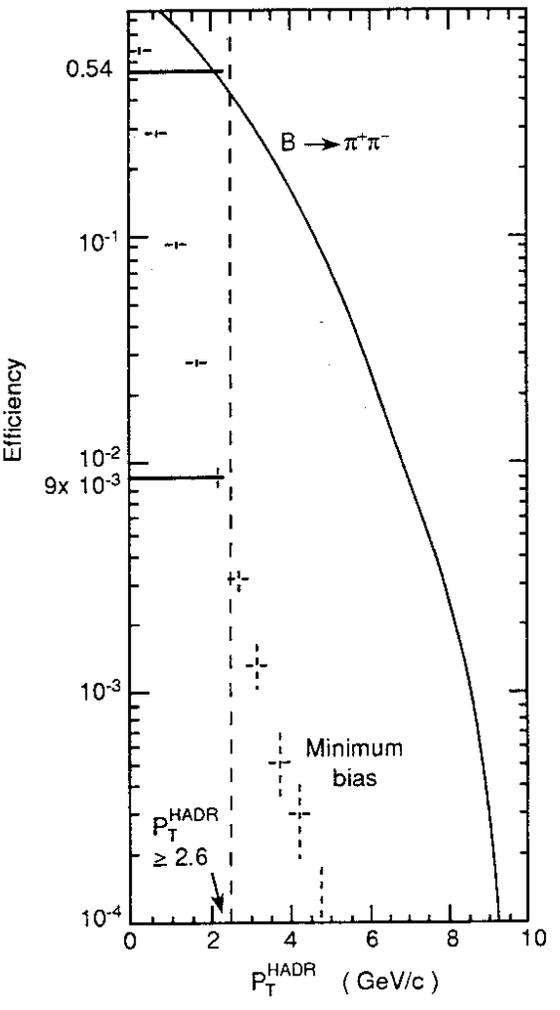

Figure 17. The efficiency of a hadronic p_T trigger as a function of the threshold on p_T^{HADR} for $B \rightarrow \pi^+\pi^-$ and minimum bias.

3.4 *Muon Trigger*

Both SFT and LHB advocate the use of three planes of Resistive Pad Chambers (RPC) for their muon trigger and Programmable Array Logic (PAL). SFT plans to use two planes between the magnet and the muon filter and one plane after the filter. For a given pad combination in chambers 1 and 3, the range of pads in chamber 2 corresponding to the minimum p_T to be triggered on is stored in the PAL.

In LHB all three RPC planes are placed behind the filter, thus reducing the occupancy (Fig. 18). Two magnets of equal and opposite deflection are used such that after the two magnets a track emerges parallel to its original direction but displaced by an amount which decreases

with increasing momentum. The trigger is therefore based on selecting 3-pad combinations that point close to the target.

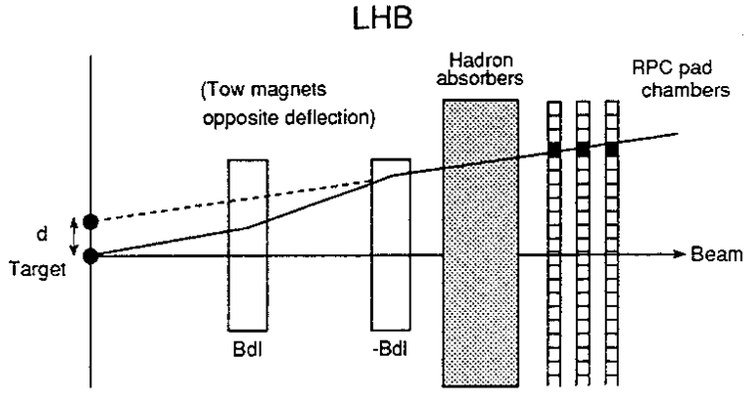

Figure 18. The LHB trigger scheme for muons.

4. COMPARISON OF SENSITIVITIES AND DIFFICULTIES

4.1 Sensitivities

The sensitivities of SFT, LHB, GAJET, and HERA B are contrasted in Table 3. The branching ratios of $B \rightarrow J/\psi K_S^0$, $J/\psi \rightarrow ,^+,^-$, and $K_S^0 \rightarrow \pi^+\pi^-$ have been taken to be 3.3×10^{-4}, 0.12, and 0.69 respectively. It is assumed that the angle β will be obtained from a time-dependent fit which minimizes the effect of oscillations in the primary B. Note that in the numbers presented by the collaborations.

- LHB has only used a lepton tag.
- HERA B, because of the very low B production cross-section, assumes a run lasting five times longer than the other proposals (but it proposes to use an existing machine!).
- There are still large differences in assumed reconstruction efficiencies (0.27 for GAJET compared with 0.57 for LHB).
- HERA B would benefit from an increase of the HERA proton energy from 0.8 TeV to 1 TeV.

Table 3. Sensitivity of SFT, LHB, GAJET, and HERA B for the $B \rightarrow J/\psi K_S^0$ channel

	SFT	LHB	GAJET	HERA
Time (s)	10^7	10^7	10^7	5.4×10^7
$b\bar{b}$	1.2×10^{10}	1×10^{10}	2×10^{10}	1.6×10^9
Hadronization	0.8	0.8	0.8	0.8
$\varepsilon_{acceptance}$ $\varepsilon_{reconstruc}$	0.30 0.66	0.52 0.57	0.4 0.27	0.08
$\varepsilon_{trigger}$	0.70	0.64	0.62	0.7
ε_{tag}	0.57	0.16	0.36 (0.14 + 0.22)	0.67
$N(J/\psi K_S^0)$	33000	6800	10440	2610
D	0.26	0.75	0.5	0.5
I		0.57	0.72	0.82
$\Delta(\sin 2\beta) = 1/(ID\sqrt{N})$	±0.021	±0.038	±0.027	±0.065 (±0.050 at 1 TeV)

Errors on sin 2β of the order of ± 0.03 could be achieved with about 10,000 observed events in one year.

The corresponding numbers for the $\pi^+\pi^-$ mode are shown in Table 4. HERA B is not proposing to investigate this channel at present. Errors on sin 2α of the order of ± 0.03 to 0.08 are anticipated.

Table 4. Sensitivity of SFT, LHB, and GAJET for the $B \rightarrow \pi^+\pi^-$ channel.

	SFT	LHB	GAJET
$\varepsilon_{acceptance}$	0.76	0.75	0.62
$\varepsilon_{reconstruc}$	0.55	0.23	0.39
$\varepsilon_{trigger}$	0.50	0.85	0.19
ε_{tag}	0.65	0.16	
$N(\pi^+\pi^-)$	2700	2200	7600
$\Delta(\sin 2\alpha)$	± 0.077	± 0.056	± 0.032

4.2 Difficulties

An attempt has been made to summarize the difficulties of the extracted beam, gas jet, and wire target approaches in Table 5. A "+" in a given column favours the corresponding method.

An extracted beam offers the advantages of a well-defined target (no surrounding halo), larger signal-to-noise ratio due to its use of a $A \neq 1$ target, better vertex resolution because of its ability to place silicon planes in the extracted beam, no beam pipe and roman pots, and smaller radiation damage. Its disadvantages are its thick target which results in multiple scattering, secondary interactions and conversions, its long target which makes triggering on secondary vertices more difficult, its increased associated multiplicity due to nuclear effects.

Table 5. Advantages (+) and disadvantages of the various fixed-target approaches to B physics.

	Extracted beam	H2 gas jet	Wire target
Well-defined target. (no diffuse gas)	+	?	+
Thin target (no sec. inter.)		+	+
$A \neq 1$	+		+
Large $\sigma_{B\bar{B}}/\sigma_{tot}$			
Assoc. mult.		+	
Target length		+	+
Easy trigger on sec. vertex (optical+silicon)		+	+
p_T trigger		+	
Vertex resolution	+		
Beam pipe and roman pots	+		
Acceptance	?		
Radiation damage	+		

A gas jet offers a thin target with no secondary interactions, a short target making secondary vertex trigger algorithms faster, a lower associated multiplicity, and a better p_T trigger. However, it has a smaller signal-to-noise ratio, worse vertex resolution, a beam pipe and roman pots, and worse radiation damage.

A wire target offers a thin target with no multiple scattering, secondary interactions or conversions, a short target making it easy to trigger on secondary vertices, and a better signal-to-noise ratio. But it has a worse associated multiplicity, a beam pipe, roman pots, and worse radiation damage.

5. CONCLUSIONS

No single method stands out as the "obvious one". An extracted beam yields better vertex resolution and an internal target easier triggering.

A flexible and diverse triggering scheme is of prime importance in order to be sensitive to as many reactions as possible; the experiment should not be limited to lepton triggers only.

Proposed experiments (P865, P867, HERA B) at existing machines will be invaluable for testing new devices and strategies for the LHC and SSC experiments.

6. ACKNOWLEDGEMENTS

The help of the members of the various collaborations, and in particular of the GAJET Collaboration, in preparing this report is gratefully acknowledged.

7. REFERENCES

1. For a review of CP violation problems see, for instance, T. Nakada, *CP Violation in K and B Meson Decays*, PSI–PR–91–02.
2. I. Dunietz, *CP Violation with Self Tagging* B_d *Modes*, CERN TH–6161/91 (1991).
3. T. Inami and C.S. Lim, *Prog. Theor. Phys.* **65** (1981) 297.
4. J.L. Hewett et al., *Phys. Rev.* **D39** (1989) 250.
5. M. Chaichian and A. Fridman, *Measurement Possibilities of CP Violation for B-Decays in* pp *Collisions*, CERN TH–6068/91 (1991);
   A. Fridman, CERN EP/90–87 (1987);
   PYTHIA, H.U. Bengtsson and T. Sjöstrand, *Comp. Phys. Commun* **46** (1987) 43.
6. S. Erhan et al., *A Dedicated Collider B Experiment, Nucl. Instrum. and Methods* **A333** (1993) 101.
7. P. Nason et al., *Nucl. Phys.* **B303** (1988) 607, **B327** (1989) 49, **B335** (1990) 260.
8. H. Akbari et al., CERN/SL/93–28 (DI), submitted to Physics Letters.
9. *An Expression of Interest in a Super Fixed Target Beauty Facility (SFT) at the Superconducting Super Collider*;
   Fixed Target B Physics at Fermilab and the SSC, S. Conetti, *Nucl. Instrum. Methods* **A333** (1993) 142.
10. F. Costantini, LHB, *Nucl. Instrum. Methods.* **A333** (1993) 125.
11. *A Measurement of Beauty Particle Lifetimes and Hadroproduction Cross-Section*, CERN SPSC 90–10, SPSC/P251 (1990).
12. *A Proposal to Study Beauty Production and other Heavy Quark Physics associated with Dimuon Production in 800 (925)* GeV/*c* pp *Interactions*, Fermilab proposal 771 (1986).
13. *Study of Two-Prong Decays of Neutral B Mesons and* Λ_b, Fermilab proposal P789 (1988).
14. *High Sensitivity Study of Charm and Beauty Decays*, Fermilab proposal P865 (1993).

15. *A Proposal to Continue the Study of Hidden Charm and Beauty States by Triggering on High Transverse Momentum Single Muons and High Mass Dimuons in 800* GeV/*c* pN *Interactions*, Fermilab proposal P867 (1993).
16. A. Bernasconi et al., Phys. Lett. **206** (1988) 163;
L. Dick and W. Kubischta, *Physics with Jet Targets at the SPS* $p\bar{p}$ *Collider in Hadronic Physics at Intermediate Energies*, ed. T. Bressani and R.A. Ricci (Elsevier Science Publishers B.V., 1986), p. 209.
17. Y. Lemoigne, *A CP Violation Gas Jet Experiment for the CERN LHC, Nucl. Inst. Meth.* **A333** (1993) 113.
18. *An Experiment to Study CP Violation in the B System Using an Internal Target at the HERA Proton Ring*, DESY PRC 92/04 (1992) and W. Hofman, *Nucl. Instrum. Methods* **A333** (1993) 153.
19. A. Fridman and B. Penzo, *Remarks about* B *Production in* pA *Collisions with a* p-*Beam of* 8 TeV, CERN PPE/91–58 (1991).
20. FRITIOF, B. Andersson et al., LU–TP–92–20 (1992).
21. J.W. Cronin et al., *Phys. Rev.* **D11** (1975) 3105.
22. K.T. McDonald, *Beam Pipes for Foward Collider Detectors,* Princeton/HEP/92–05 (1992).
23. L. Rossi, private communication.
24. *Study of Beauty Physics at the SPS Collider with Real Time Use of Silicon Microvertex Information*, CERN SPSC/88–33, 89–43, 89–55 and 89`–61, SPSC/P238, and J. Ellett et al., *Nucl. Instrum. Methods* **A317** (1992) 28.
25. G. Carboni, *Radiation Damage to Microvertex Detectors*, LHB–Note–1 (1991).
26. G. Hall, *Radiation Resistance of Semiconductor Detectors and Associated Electronics,* in *Proceedings of the Large Hadron Collider* Workshop, Aachen 1990, eds. G. Jarlskog and D. Rein, CERN 90–10 (1990) Vol. III, p. 693, .
27. *Integrated High Rate Transition Radiation Detector and Tracking Chamber for the LHC*, CERN/DRDC/90–38, DRDC/P8 (1990).
28. *Study of Optical Trigger to be used for Beauty Search in Fixed Target Mode at LHC,* CERN DRDC 91–32 and 92–53, G. Charpak et al., *Nucl. Instrum. Methods* **A306** (1991) 439.
29. G. Charpak et al., *Nucl. Instrum. Methods* **A332** (1993) 91.